Stability and Reactivity of Molecules Encapsulated in a Carbon Nanotube. A Variable-Temperature Variable-Voltage Transmission Electron Microscopic Study

Dongxin Liu,[†] Satori Kowashi,[†] Takayuki Nakamuro,*,[†] Dominik Lungerich,[†,‡, ‖] Kaoru Yamanouchi,[†] Koji Harano,*,[†] Eiichi Nakamura*,[†]

[†]Department of Chemistry, The University of Tokyo, 7-3-1 Hongo, Bunkyo-ku, Tokyo 113-0033, Japan

[‡]Center for Nanomedicine (CNM), Institute for Basic Science (IBS), IBS Hall, 50 Yonsei-ro, Seodaemun-gu, Seoul, 03722, South Korea.

[‖]Graduate Program of Nano Biomedical Engineering (NanoBME), Advanced Science Institute, Yonsei University, Seoul, 03722, South Korea.

ABSTRACT:

Transmission electron microscopy has suffered from information loss during observation often ascribed to the structural changes of a specimen into a different substance, known as radiation damage. The damage in organic matters predominantly occurs via ionization (radiolysis). Although radiolysis is highly important, studies on radiolysis have largely been descriptive and qualitative, because of the complexity of the process and the difficulty to quantify the changes under variable temperature and variable acceleration voltage (VT/VV) conditions. We report here the kinetic study of the dimerization of a van der Waals dimer [60]fullerene (C_{60}) into C_{120} in carbon nanotube (CNT), in which we found five competing reaction pathways that serve as model pathways of radiolysis damage. We found marked influence of the temperature, the acceleration voltage, and the properties of the CNT, and reaction paths have been distinguished by the pre-exponential factor and the Arrhenius activation energy. The most frequently occurring reaction took place via singlet (S_1) or triplet (T_1) species generated by energy transfer from CNT exciton. We found an experimental model on how CNT protects the specimen from radiolysis, which accounts for the stability of a variety of molecules having low-lying HOMOs. We also observed a radiolysis pathway taking place in a heavily damaged CNT. The triplet reaction also occurs when we use an oxidized CNT which is known to form a triplet exciton. The VT/VV behavior of the kinetics agrees with the competitive occurrence of electron excitation and ionization but not with the atomic displacement damage mechanism. The complexity of the kinetics suggests a risk in making any mechanistic interpretations of chemical events seen by TEM without performing VT/VV kinetic analysis. The result provides an illustration of the potential of atomic resolution video imaging of chemical events for elucidation of the mechanisms of chemical reactions.

INTRODUCTION

Since the time of the Knoll/Ruska invention of transmission electron microscopy (TEM),[1] electron microscopy has suffered from information loss during observation often ascribed to the structural changes of a specimen into a different substance, known as radiation damage.[2] As summarized recently by Egerton,[3] the electron-beam (e-beam) damage in organic matters predominantly occurs via processes triggered by ionization (radiolysis). Although radiolysis is highly important, studies on radiolysis have largely been descriptive and qualitative, because of the complexity of the process and the difficulty to quantify the changes under variable temperature and variable acceleration voltage (VT/VV) conditions. The first step of the process involves electron-impact ionization (EII) that removes an electron to form a radical cation (RC) of the specimen, or possibly also electron-impact excitation (EIE) where the electron does not fly away to the vacuum but stays in a higher antibonding state in the system. The processes were recently studied in depth for the first time by a thorough quantum chemical study.[4] There has been, however, a paucity of experimental mechanistic

information; that is, how a specimen is transformed to what product with what level of activation energy and frequency at what acceleration voltage. A number of single molecules encapsulated in a carbon nanotube (CNT) have been observed either stably or undergoing well-defined chemical transformations,[5,6,7,8,9] primarily because the damage due to secondary electrons is minimum.[10] Drawing an analogy between metal and quasi-1-D CNT for their conductivity and electron-donating ability (Figure 1a), we suspect that CNT protects the molecule from ionization by filling in the electron vacancy in the RC. Specimen stabilization by a thin metallic coating or deposition on a conductive indium tin oxide substrate in scanning electron microscopy (SEM) has been well documented.[11] In light of the recent characterization of singlet and triplet excitons of CNTs (Figure 1a),[12] we conjectured also that the CNT exciton would excite a molecule in the CNT via energy transfer (ENT)[13,14] (Figure 2a). Electron excitation of graphene under TEM conditions has also been suggested recently.[15,16].

We report here the VT/VV kinetic study of the dimerization of a van der Waals (vdW) dimer [60]fullerene (C_{60}) into C_{120} in

CNT,[17,18,19] in which we found five competing reaction pathways that serve as model pathways of radiolysis damage (Figure 1b-f). We found marked influence of the temperature, the acceleration voltage, and the properties of the CNT—pristine (prCNT), oxidized (oxCNT), or damaged CNT (dmCNT) (Figure 2b). They have been distinguished by the pre-exponential factor (PEF) and the Arrhenius activation energy (E_a). The most frequently occurring reaction was found to occur via singlet (S_1) or triplet (T_1) species generated by energy transfer (ET) from CNT exciton (Figure 1b,c).[3] Electrons of 60 keV in energy cannot energize prCNT to the triplet state, and instead ionizes directly C_{60} into RC that is then reduced by the CNT to a mixture of S_1 and T_1 (Figure 1d). This process illustrates how prCNT protects the specimen from radiolysis (Figure 2c), and accounts for the stability of a variety of molecules having low-lying HOMOs, such as saturated hydrocarbons,[20] amides,[21] alcohols,[22] and inorganic salts encapsulated in a CNT.[23,24]

We observed RC, when the reaction was performed in a heavily damaged CNT (Figure 1e). The triplet reaction also occurs when we use an oxidized CNT, which is known to form a triplet exciton (Figure 1f). The VT/VV behavior of the kinetics agrees with the competitive occurrence of electron excitation and ionization, but not with the atomic displacement damage mechanism, which has been seen only in conductive inorganic materials.[25]
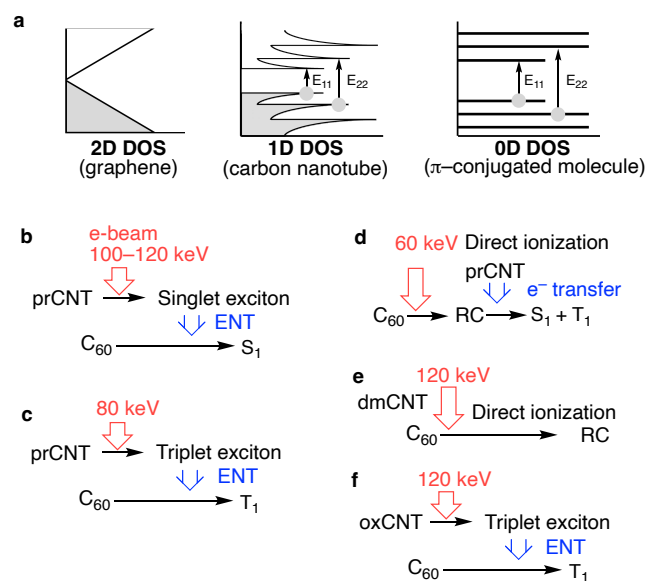
2D DOS
(graphene)

1D DOS
(carbon nanotube)

0D DOS
(π–conjugated molecule)

b
e-beam
100–120 keV
prCNT → Singlet exciton
C_{60} → S_1 (ENT)

c
80 keV
prCNT → Triplet exciton
C_{60} → T_1 (ENT)

d
60 keV Direct ionization
prCNT
C_{60} → RC → $S_1 + T_1$ (e⁻ transfer)

e
120 keV
dmCNT Direct ionization
C_{60} → RC

f
120 keV
oxCNT → Triplet exciton
C_{60} → T_1 (ENT)

Figure 1. Density of states (DOS) and pathways of C_{60} excitation. (a) DOS of 0-D to 2-D materials. (b–f) CNT excitation by EIE and ENT from CNT to C_{60}.
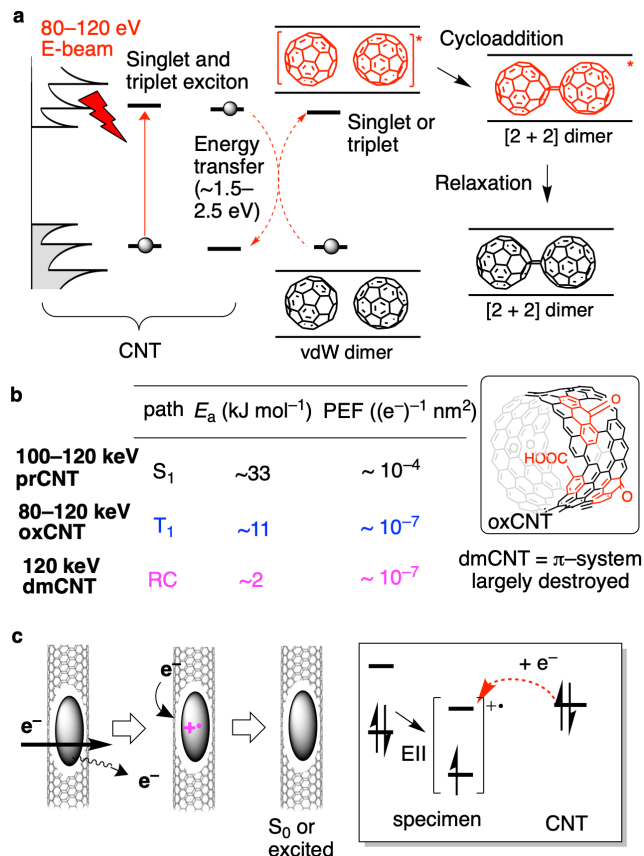
a
80–120 eV E-beam
Singlet and triplet exciton
Energy transfer (~1.5–2.5 eV)
Singlet or triplet
Cycloaddition
[2 + 2] dimer
Relaxation
[2 + 2] dimer
CNT
vdW dimer

b

path	E_a (kJ mol⁻¹)	PEF ((e⁻)⁻¹ nm²)
100–120 keV prCNT — S_1	~33	~ 10^{-4}
80–120 keV oxCNT — T_1	~11	~ 10^{-7}
120 keV dmCNT — RC	~2	~ 10^{-7}

oxCNT
HOOC

dmCNT = π–system largely destroyed

c
e⁻
EII
S_0 or excited
+ e⁻
specimen
CNT

Figure 2. Electron-impact promoted [2 + 2] cycloaddition mediated by CNT–quasi-1D material. (a) [2 + 2] Dimerization of C_{60} by EIE of the CNT followed by ENT from the CNT exciton to C_{60}. The E_{22} transition is shown as a simplified example of transitions responsible for the C_{60} excitation. (b) Representative kinetic parameters of C_{60} dimerization under VT/VV conditions. (c) Neutralization of an ionized specimen molecule by electron transfer from the prCNT.

RESULTS

Light transfers its energy to a zero-dimensional (0D) material via an electric dipole transition (EDT) mechanism with conservation of spin angular momentum (Figure 1a),[26] and the excited species undergo intersystem crossing (ISC)[27] and ENT.[28] Being a particle wave, e-beam lacks EDT capability, and causes predominantly plasmon excitation, EII, and atom displacement via momentum transfer.[29] EIE of CNT occurs with conservation of spin angular momentum.[30] CNT resembles 0D materials due to van Hove singularities (Figure 1a),[31] and we envisaged that the CNT exciton transfers energy to C_{60} encapsulated in CNT (Figure 2a). We monitored the reaction using single-molecule atomic-resolution time-resolved electron microscopic technique (SMART-EM) under VT/VV conditions at 103–493 K and 60–120 keV.[10,19]

The thermally forbidden [2 + 2] dimerization of vdW $(C_{60})_2$ does not take place at temperatures <800 K.[32] The reaction commences upon photo-irradiation of C_{60} film or solid,[33,34] also occurs upon electron irradiation (Figure 2a, box). Further irradiation converts the initially formed [2 + 2] dimer eventually to a

short CNT[18] via retro [2 + 2] cycloaddition and a series of Stone–Wales rearrangements (Figure 3a).[35]

In 2011, C_{60} dimerization in CNTs was reported to take place even with 20 keV irradiation, although it then requires a 100-times larger electron dose that at 80 kV.[36] The 20 keV energy is far lower than the threshold voltage of carbon atom displacement (CAD, knock-on displacement), and the data suggests a mechanism not going through CAD. A 60-keV electron beam was recently reported to cause reactions of C_{60} sandwiched between two graphene sheets – loss of one carbon atom to form a C_{118} (quasi) dimer via C_{59}.[37] This may suggest a difference between a 1D CNT and gapless 2D graphene that lacks van Hove singularities (Figure 1a). This is briefly examined in the present study.
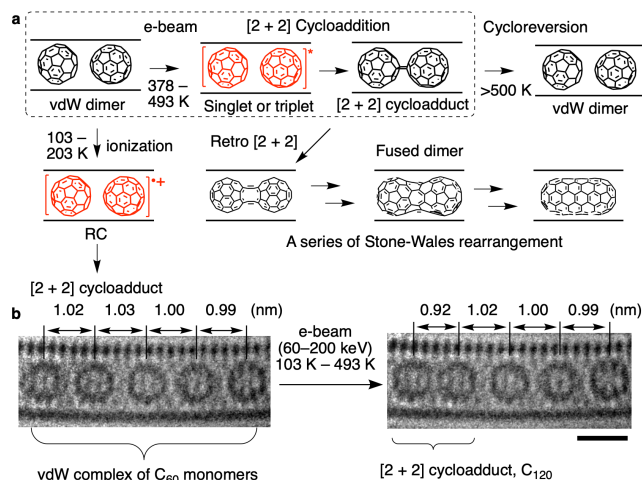
Figure 3. [2 + 2] Cycloaddition via excited state. (a) Cycloaddition via excited state and RC as well as retro cycloaddition and further fusion to produce a short CNT. (b) TEM images of vdW complexes (intermolecular distance 0.99–1.03 Å) and [2 + 2] dimer (0.92 Å). Fused dimer in (a) shows a characteristic intermolecular distance of 0.8 Å. Scale bar = 1 nm.

VT-SMART-EM imaging is an emerging experimental tool for the study of kinetics and thermodynamics of individual chemical events,[19,22,38] and it has provided direct experimental proof of the Rice–Ramsperger–Kassel–Marcus theory.[39] In this study, we performed VT-SMART-EM imaging under VV conditions (VT/VV-SMART-EM). Following the reaction conditions developed previously,[19] we encapsulated the fullerene molecule in a bundle of pr-, ox-, or dmCNTs, 1.3–1.4 nm in diameter,[40] by heating them together at 823 K for 15 h in vacuo. A specimen was deposited on a TEM grid and the time evolution of the [2 + 2] cycloaddition of a $(C_{60})_2$@CNT was visually monitored with a frame rate of two frames per second (s) under e-beam irradiation at 120, 100, 80, and 60 kV, with a constant electron dose rate (EDR) of 3.1×10^5 e^- nm^{-2} s^{-1} for 120 kV and 5.0×10^6 e^- nm^{-2} s^{-1} for 60–100 kV throughout this study. Note that the reaction rate per electron measured in the present work is not affected by the variation of EDR as previously reported.[19]

The cycloaddition event was characterized by the change in intermolecular distance from 1.00 nm for the vdW dimer to 0.90 nm for the cycloadduct (Figure 3b), and the E_a and PEF were determined.[19] The [2 + 2] cycloadduct features a strained cyclobutane ring in the middle and reverts to two molecules of C_{60} upon heating at >500 K, thus providing compelling chemical evidence that the adduct is the C_{120} cycloadduct (Figure 3a).
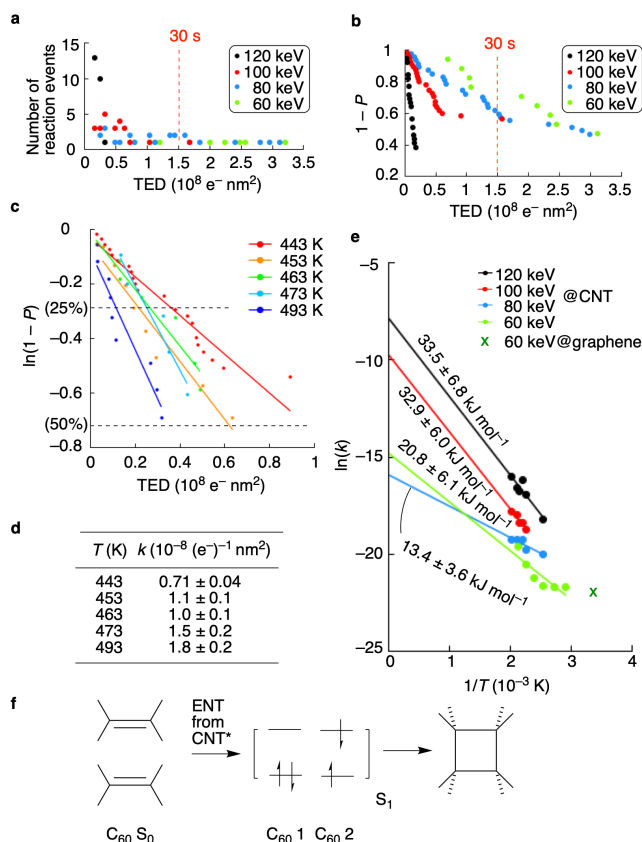

Figure 4. VT/VV-SMART-EM kinetic study of C_{60} dimerization. (a) Occurrence of stochastic reaction events of C_{60} dimerization integrated over every 8.0×10^6 e^- nm^{-2} at 443 K plotted against TED (Table S3, Figure S2). (b) Reaction progress of C_{60} dimerization at 443 K. (c) Semilogarithmic plot of C_{60} dimerization at 100 kV above 443 K and first-order kinetic fitting shown as solid lines. (d) Reaction rate constants of C_{60} dimerization at 100 kV obtained via linear fitting of (c). (e) Arrhenius plot of C_{60} dimerization. The green plot is for the 60-keV reaction, where the slope at higher temperature ($1/T = 2$ to 2.4×10^{-3}) is close to that of the S_1 path (black, red) and that at lower temperature (2.5 to 3×10^{-3}) is close to the T_1 path (blue). The x indicates the $\ln(k)$ value for dimerization of C_{60} sandwiched between graphene sheets estimated from Figure 4 in ref 37. (f) Mechanistic sketch of the S_1 cycloaddition.

Singlet Dimerization of a $(C_{60})_2$@CNT

Unlike light that can transfer its entire energy for electron excitation of molecules via an EDT mechanism, the momentum transfer mechanism of an e-beam can transfer its energy to molecules very inefficiently. To assess how inefficient it would be, and to know the consequence of poor efficiency, we performed the kinetic analysis at an acceleration voltage decreasing stepwise from 120 keV to 60 keV.

We first found that a beam of 100–120 keV electrons excites a $(C_{60})_2$ vdW dimer to the S_1 state – a pathway expected because the EIE with high-energy e-beam occurs with conservation of spin angular momentum.[30] Rather unexpectedly, however, the S_1 path was unavailable with a beam of 80-keV electron, which instead opened a T_1 path, suggesting that the 80-keV electron generated a triplet CNT exciton. ISC from a singlet exciton of CNT to triplet was documented recently.[12] Given the reported S_0/S_1 energy difference of ~2.5 eV for C_{60},[41] we estimated that the 100–120 keV e-beam transferred at most ~2.5 eV to C_{60},

that is, 2 to 2.5×10^{-5} of its kinetic energy (2.5 eV/100–120 keV). Similarly, the S_0/T_1 energy difference of ~1.5 eV for C_{60}[41] suggests that at most ~1.9×10^{-5} of the 80 keV was utilized for C_{60} excitation.

Taking these numbers at 80–120 keV into account, we expect that a beam of 60 keV electrons cannot excite the CNT, which typically has a bandgap of 1 eV, and hence we expect no dimerization at 60 keV. Interestingly, excited-state dimerization at 60 keV did take place, albeit very infrequently, suggesting that the excited states are not generated via ENT from the CNT but via the RC (Figure 1d).

In Figure 4, we summarize all the data of the dimerization at 60–120 keV at 443–493 K. The raw data at 443 K are shown in Figure 4a, where we plot the number of dimerization events observed at intervals of 8.0×10^6 e$^-$ nm^{-2} irradiation against the total electron dose (TED) up to 3.0×10^8 e$^-$ nm^{-2} (for 60 s). After in situ monitoring of the reactions of 39–55 C_{60} dimerization events at acceleration voltages of 120 (black), 100 (red), 80 (blue), and 60 kV (green, Figure 4a), we observed three features. First, each reaction event takes place stochastically.[42] Second, the occurrence of the events follows the first-order kinetics shown in Figure 4b and c, where the $1 - P$ and $\ln(1 - P)$ values are plotted against TED (P = normalized conversion of C_{60}). Third, we find three different kinetic profiles.

The rate constants (k) at 100 kV are summarized in Figure 4d. The error is arguably large, for several reasons. The CNT is a mixture of entities having different chirality indexes (i.e., the diameters)[43] and, under different physicochemical environments, molecular packing in CNTs changes as the reaction proceeds.

Using the rate constants k obtained at five temperatures, we plotted the Arrhenius plot to obtain the activation energy (E_a, slope) and PEF (y-intercept) (Figure 4e). The E_a values at 120 and 100 kV are nearly identical, 33.5 ± 6.8 and 32.9 ± 6.0 kJ mol^{-1}, respectively, hence suggesting the same reaction mechanism. The reaction in CNTs under 120 kV (PEF = 3.9×10^{-4} (e$^-$)$^{-1}$ nm^2) occurs more frequently than the reaction under 100 kV (PEF = 5.9×10^{-5} (e$^-$)$^{-1}$ nm^2).

The reaction at 80 kV took place with E_a and PEF values essentially the same as those of the T_1 reaction mediated by a triplet-sensitizing oxCNT (see below). We therefore consider the reaction to take place via T_1. The T_1 species forms less frequently (y-intercept = PEF) but is more reactive than the S_1 species (slope = E_a). An orbital diagram of the concerted singlet cycloaddition is illustrated in Figure 4f.

The reaction at 60 kV was markedly slower at ~400 K than the reaction at 100–120 kV (Figure 4b and Figure S3). The Arrhenius plot (green, Figure 4e) deviates from linearity, and we surmise that the kinetics reflects competing S_1 and T_1, generated by direct EIE and not mediated by the CNT (Figure 2c; see below). Indeed, the estimated E_a value of 20.8 ± 6.1 kJ mol^{-1} and PEF = 3.7×10^{-7} (e$^-$)$^{-1}$ nm^2 fall between the values of pure S_1 and pure T_1.

We estimated the reaction rate of the recently reported dimerization of C_{60} sandwiched between two graphene sheets at 60 kV (Figure 4e caption),[37] and obtained $\ln(k) = -21.9$. This data placed at 298 K in Figure 4e (dark green, x) lies close to our 60-kV data.

Triplet Dimerization of a $(C_{60})_2$@oxCNT

The oxCNT (Figure 2b), prepared using KMnO$_4$ oxidation of a CNT,[44] has both the π- and σ-carbon skeletons destroyed by chemical oxidation, as demonstrated by infrared (IR) absorption (due to benzophenone-like groups).[45] It is reported to be a triplet sensitizer in solution, as efficient as benzophenone, and has a triplet energy lower than ~2.5 eV.[46] We encapsulated C_{60} in oxCNT and studied 30–52 vdW C_{60} dimers $((C_{60})_2$@oxCNT).

The time course of the dimerization events at 120 kV, with a constant EDR of 3.1×10^5 e$^-$ nm^{-2} s^{-1}, is shown in Figure 5a, and the frequency integrated over time in Figure 5b. The semi-logarithmic plot in Figure 5c gives the reaction rates at temperatures between 378 and 453 K, and the Arrhenius plot gives the E_a and PEF values (Figure 5d). The data agree with values obtained for a prCNT at 80 kV (Figure 4e), suggesting a triplet mechanism (Figure 5e).
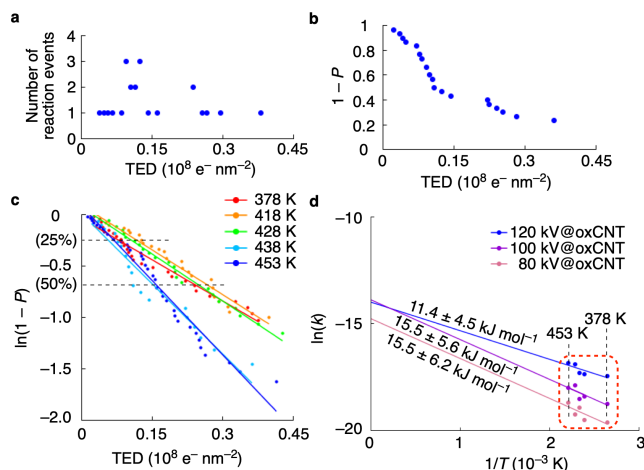

Figure 5. Kinetic study of C_{60} dimerization in an oxCNT. (a) Occurrence of stochastic reaction events of C_{60} dimerization inside oxCNTs at 120 kV integrated over every 8.0×10^6 e$^-$ nm^{-2} at 438 K for a $(C_{60})_2$@oxCNT plotted against TED (Table S4, Figure S4-5). (b) Reaction progress of C_{60} dimerization inside oxCNTs at 120 kV. (c) First-order kinetics of C_{60} dimerization inside oxCNTs at 120 kV. (d) Arrhenius plot of C_{60} dimerization inside oxCNTs at 80–120 kV. (e) Mechanistic sketch of the T_1 reaction.

C_{60} dimerization at 103–203 K occurred with induction period (Figure 6c),[19] during which the π-conjugation of the CNTs was destroyed, as seen in Figure 6a and b.[47] After the induction period, a steady first-order reaction took place. We measured the reaction rate and obtained $E_a = 1.7 \pm 0.6$ kJ mol^{-1} and PEF = 1.3×10^{-7} (e$^-$)$^{-1}$ nm^2 (Figure 6d).

The remarkably low E_a value suggests an RC, which is formed by ionization and is expected to be extremely reactive (Figure 6e). RC formation is expected by the standard damage mechanism of radiolysis.[3]
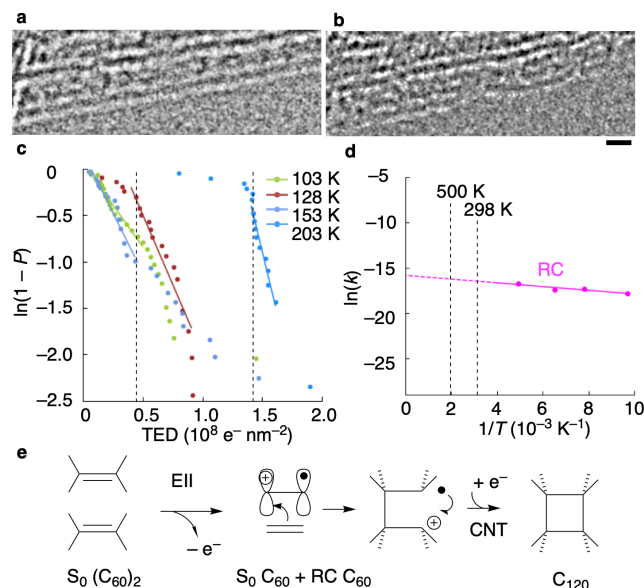
Figure 6. Dimerization at 103–203 K via RC. (a,b) The C_{60}@prCNT decomposes after prolonged irradiation at 153 K to produce C_{60}@dmCNT. Scale bar = 1 nm. (c) First-order kinetics of C_{60} dimerization in dmCNTs at 120 kV. Dotted lines show the end of induction period at 128 K and 203 K, from where the rate was calculated. (d) Arrhenius plot of C_{60} dimerization in a dmCNT at 120 kV. (e) Mechanistic sketch of the RC reaction.

Table 1 summarizes the E_a and PEF data in pr-, ox-, and dmCNTs of the four reaction types (Figure 1b–e). The kinetic profiles are color coded in black, blue, green, and purple. We consider that the path with E_a values of 32.9–33.5 ± ~6 kJ mol⁻¹ in Table 1a (black) took place via S_1, first because a high-energy e-beam excites CNT with conservation of spin angular momentum, and second because the values compare favorably (within experimental error) with an E_a value of 28 kJ mol⁻¹ reported theoretically for S_1 [2 + 2] cycloaddition in gas phase.[48] We assign the E_a values of 11–15 kJ mol⁻¹ in Table 1b as obtained for the oxCNT to the T_1 pathway[41] because an oxCNT is an effective triplet sensitizer due to aromatic ketone residues that accelerate relaxation of singlet to triplet.[49] The low values of E_a agree with the biradical character of the T_1 excited state of C_{60}. Similarly, we assign T_1 to the 80-keV experiment in a prCNT (Table 1a) because the kinetic data agree with those for an oxCNT in Table 1b. The value of 20.8 kJ mol⁻¹ at 60 keV in Table 1a (green) coincides with a value of 23 kJ mol⁻¹ determined for photodimerization possibly reflecting ISC from singlet to triplet possibly in a 1:3 ratio.[50]

Table 1. E_a and PEF values obtained from the Arrhenius plot of the C_{60} dimerization events: (a) C_{60} dimerization in a prCNT, (b) in a oxCNT, and (c) in a dmCNT. Color coding according to the reactive species.

a $(C_{60})_2$@prCNT

e-beam (keV)	E_a (kJ mol⁻¹)	ln(PEF)	PEF ((e⁻)⁻¹ nm²)	path
120	33.5 ± 6.8	−7.9 ± 1.8	3.9×10^{-4}	S_1
100	32.9 ± 6.0	−9.7 ± 1.6	5.9×10^{-5}	S_1
80	13.4 ± 3.6	−15.9 ± 1.0	1.2×10^{-7}	T_1
60	20.8 ± 6.1	−14.8 ± 1.8	3.7×10^{-7}	S_1/T_1

b $(C_{60})_2$@oxCNT

e-beam (keV)	E_a (kJ mol⁻¹)	ln(PEF)	PEF ((e⁻)⁻¹ nm²)	path
120	11.4 ± 4.5	−14.0 ± 1.3	8.3×10^{-7}	T_1
100	15.5 ± 5.6	−13.9 ± 1.9	9.3×10^{-7}	T_1
80	15.5 ± 6.2	−14.8 ± 1.8	3.9×10^{-7}	T_1

c $(C_{60})_2$@dmCNT

e-beam (keV)	E_a (kJ mol⁻¹)	ln(PEF)	PEF ((e⁻)⁻¹ nm²)	path
120	1.7 ± 0.6	−15.9 ± 0.5	1.3×10^{-7}	RC

DISCUSSION

The SMART-EM study on the electron-impact promoted [2 + 2] cycloaddition mediated by CNTs (Figure 7) is unique in that we can study in situ the individual reaction events one by one as they take place. The first stage is a fast EIE reaction, characterized by the PEF data. The second stage is a slow thermally driven reaction of excited C_{60} going across an energy barrier with a frequency of $\exp(-E_a/RT)$. We determined the kinetic parameters separately for the two steps by visually monitoring the individual events of the forward cycloaddition of vdW complexes, which excludes the contribution of cycloreversion and reversible collisions from the kinetic data analysis.
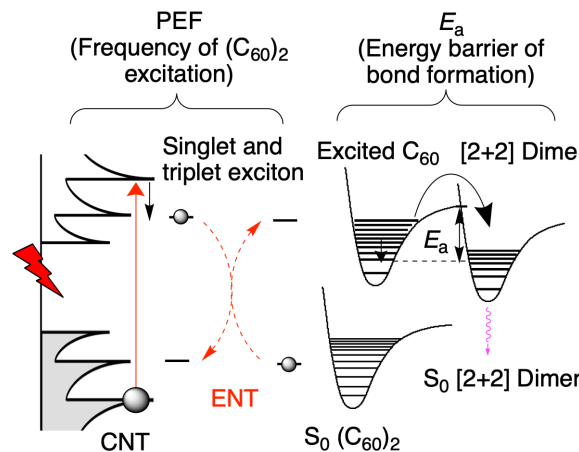

Figure 7. PEF and E_a, representing EIE/ENT and cycloaddition, respectively. Of two possible mechanisms of ENT, the Förster mechanism of ENT is shown. The E_{22} transition is shown as an example of transitions responsible for C_{60} excitation. The E_{33} transition followed by thermal relaxation is shown as an example of the processes involved in the C_{60} excitation.

The ln(PEF) values represent ln(k) at T = infinite, and they vary widely between −7.9 and −16.4 (PEF = $3.9 \times 10^{-4} - 1.3 \times 10^{-7}$ (e⁻)⁻¹ nm²). They are also extremely low in absolute magnitude, indicating that a large number of electrons ($1.0 \times 10^3 - 3.0 \times 10^6$ electrons) are required to form one excited or ionized C_{60} molecule (area of 0.396 nm²) that produces the dimer. The E_a values

(slope) reflect the reactivity of these species in the thermal dimerization reaction (Figure 7, second step).

To describe the efficiency of the reaction, we borrow the concept of external quantum efficiency (EQE) used to evaluate the efficiency of photovoltaic devices—the ratio of the number of electrons and holes generated by a device to the number of incident photons shining on the device from outside. Similarly, we can define the EQE based on the number of dimers formed relative to the TED shining on the CNT. The EQE values of the S_1 reaction in a prCNT and the T_1 reaction in an oxCNT at 120 kV are 9.8×10^{-4} and 2.1×10^{-6}, respectively, indicating that the latter is nearly 1000 times less efficient because of the infrequent formation of the triplet exciton of the CNT. The very low value of the energy attenuation factor (~10^{-5}; from ~100 keV to ~2 eV) reflects the lack of a mechanism for efficient energy transfer from the e-beam to the CNT and the loss of energy to phonon vibration of the CNT and physicochemical processes.
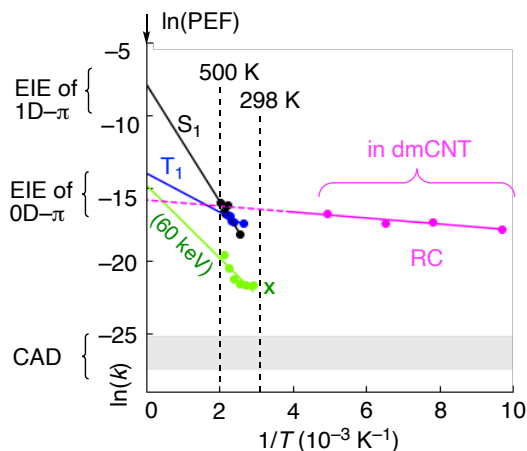

Figure 8. Arrhenius plot for four representative reactions. Black: The 120 kV data in Table 1a via S_1. Blue: the 120 kV data in Table 1b via T_1. Green: the 60 kV data in Table 1a via direct EIE. Purple: the 120 kV data in Table 1c via RC. Gray band: a range of $\ln(k)$ values for temperature-independent CAD estimated from $\ln$(PEF) of radiolysis. The x indicates the $\ln(k)$ value for dimerization of C_{60} sandwiched between graphene sheets estimated from Figure 4 in ref 37.

The Arrhenius plots for the four representative reactions in Figure 8 summarize the present finding. In accordance with the accepted mechanism of radiation damage, the ionization pathway operates in dmCNT (purple). In prCNT encapsulating C_{60} (at >300 K), the ionization is suppressed, and much faster excited-state pathways dominate when the energy of the e-beam is >80 keV (black and blue). When the e-beam energy is 60 keV, it does not excite the CNT and hence C_{60}.
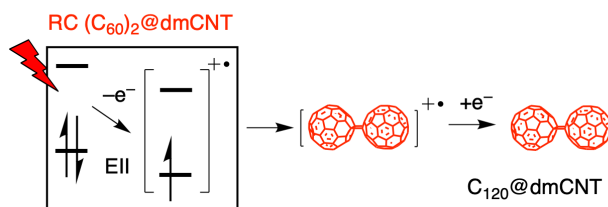
The S_1 species forms in the reaction of C_{60}@prCNT at 120 kV (black) that took place most frequently (the largest $\ln$(PEF) value of –7.9). The other three pathways via EIE or EII occurred ~500 times less frequently. Extremely reactive RC (purple) reacted with near-zero E_a and very small $\ln$(PEF) = –15.9.[51] We estimate the $\ln$(PEF) of CAD of C_{60} to be ~–25 to –27, shown as a gray band in Figure 8, based on the $\ln$(PEF) of RC and the reported frequency difference of ~10^5 between CAD and radiolysis of polymers.[52] Because CAD is temperature independent,[37] we estimate $\ln(k)$ to be ~–25 to –27. Thus, the carbon loss of C_{60} would occur approximately 10^{-5} times more slowly than that of the excited-state reactions. We thus expect CAD to

become noticeable only after irradiation with TED of 10^9–10^{11}, a dose 100 times greater than that used for SMART-EM imaging. The probability of the atom displacement depends on the collision cross section, which decreases as the atomic number decreases.
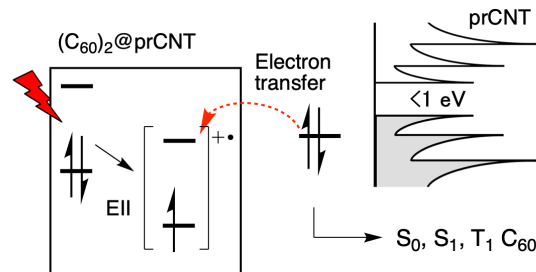
Figure 9 illustrates the orbital diagrams of the reaction pathways identified in the present study. Figure 9a shows ionization the π-rich C_{60}, the standard mechanism of radiation damage (Figure 1e).[52] We found this path at 103–203 K in a dmCNT, and consider that it also account for the CNT damage at low temperatures (cf. Figure 6a,b). Figure 9a-2 illustrates C_{60} ionization followed by charge neutralization by prCNT and generation of S_0, S_1, or T_1 C_{60} (Figure 1d). We observed this path at 60 kV.[36] On the other hand, 100–120 keV electron is energetic enough to generate singlet exciton of CNT, and energy transfer forms S_1 C_{60} (Figure 1b), while 80 keV electron forms T_1 C_{60} (Figure 1c). In Figure 9c, ox-CNT generates triplet exciton of CNT, which transfers energy to form T_1 C_{60} (Figure 1f).
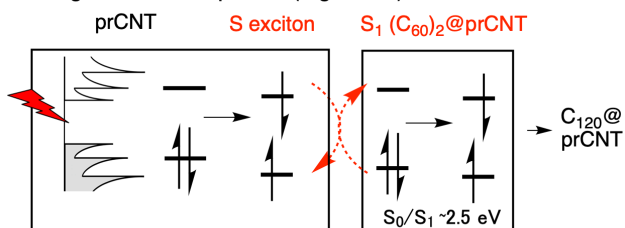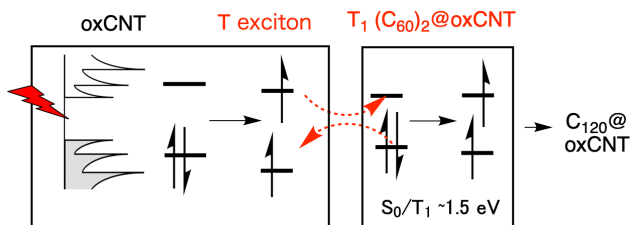

Figure 9. Four pathways available for activation of vdW $(C_{60})_2$@CNT for [2 + 2] cycloaddition. (a) Two paths following the initial ionization. (a-1) Ionization of C_{60} to generate radical

cation at 103–203 K in a dmCNT. (a-2) Ionization of C_{60} followed by charge neutralization to generate an excited state taking place with a 60-kV e-beam. (b) Singlet CNT exciton generates S_1 C_{60} with a 100 to 120-kV e-beam. (c) Triplet oxCNT generates T_1 C_{60} with an 80-kV e-beam.

CONCLUSION

In summary, the kinetics data summarized in Figure 8 have shown that the conducting prCNT with its high-lying filled orbital protects the molecule from radiolysis[8] by neutralizing RCs formed by direct EII (Figure 2c). The data account for the unexpectedly higher stability of molecules in conductive CNT than those in bulk.[8] Prevention of ionization by coating the specimen with conductive material is a common practice in SEM, and graphene sheets may function similarly.[15] If a suitable reaction mechanism is available, an e-beam can bring π-electron-rich molecules into excited states of finite lifetime, and this process will change the structure of the specimen such as the conversion of C_{60} into a dimer—a process to be viewed as a damage process controlled by a conducting substrate. The complexity of the kinetics of EII and EIE suggests a risk in making any mechanistic interpretations of chemical events seen by TEM without performing VT/VV kinetic analysis. Here we have provided an additional illustration of the potential of video imaging of chemical events, "cinematic chemistry", for elucidation of the mechanisms of chemical reactions.[40]

EXPERIMENTAL SECTION

Materials Single-walled carbon nanotubes (CNTs, Meijo Arc SO, produced by arc-discharge using Ni and Y catalysts, >99% purity, average diameter 1.4 nm, Lot # 6601316) were purchased from Meijo Nano Carbon Co. Ltd. C_{60} powder (nanom purple ST, >98% purity) was purchased from Frontier Carbon Corporation. TEM grids precoated with a lacey microgrid (RO-C15, for VT experiments; pore size 3–8 μm and carbon thickness 70 nm) were purchased from Okenshoji Co., Ltd. Toluene was purchased from Wako Pure Chemical Industries and purified using a solvent purification system (GlassContour)[53] equipped with columns of activated alumina and supported copper catalyst (Q-5) prior to use. Potassium permanganate was purchased from Tokyo Chemical Industry Co., Ltd and sulfuric acid was purchased from Wako Pure Chemical Industries.

General The water content of the solvent was determined using a Karl Fischer moisture titrator (CA-21, Mitsubishi) to be <10 ppm. Bath sonication for the dispersion of CNTs in toluene was carried out with a Honda Electronics WT-200-M instrument. Oxidative removal of the terminal caps of CNTs was carried out in an electric furnace ASH ARF-30KC. Encapsulation of C_{60} into CNTs was carried out in an electric furnace ASH AMF-20, equipped with a temperature controller AMF-9P. IR spectra were recorded on a JASCO FT/IR-6100 instrument with attenuated total reflection. X-ray photoelectron spectroscopy analysis was carried out on a JPS-9010MC instrument using Mg Kα X-rays (1253.6 eV).

Preparation of samples for SMART-EM The C_{60}@CNTs prepared above are in solid form and thus difficult to deposit directly on a TEM microgrid. We therefore first dispersed samples in toluene (0.01 mg/mL), in vials, which were then placed in a bath sonicator for 1 h. The aim was to soften the samples

so that we could secure intimate contact between the CNTs and the carbon surface of the grid. A 10 μL solution of the dispersion was then deposited on a TEM grid placed on a paper that absorbs excess toluene. The resulting TEM grid was dried in vacuo (60 Pa) for 2 h.

SMART-EM observation Atomic-resolution TEM observations were carried out on a JEOL JEM-ARM200F instrument equipped with an aberration corrector and cold-field emission gun (point resolution 0.10 nm) at acceleration voltages of $E = $ 60, 80, 100, and 120 kV, under 1×10^{-5} Pa in the specimen column, and with typical spherical aberration values of 1–3 mm. Calibration of the EDR was conducted following a method described in a previous report.[19] C_{60} dimerization at 60–120 kV and C_{60} dimerization in oxCNT were monitored at the temperatures mentioned in the main text and an EDR (the number of electrons per second per nm^2) of ca. 3.1×10^5 e^- nm^{-2} s^{-1} for 120 kV and 5.0×10^6 e^- nm^{-2} s^{-1} for 60–100 kV at 800,000× magnification. The imaging instrument was a CMOS camera (Gatan OneView, 4,096 × 4,096 pixels), operated in binning 2 mode (output image size 2,048 × 2,048 pixels, pixel resolution 0.20 nm at 1,000,000×). A series of TEM images was recorded every 0.5 s as a superposition of 25 consecutive images of 0.04-s frames (automatically processed on Gatan DigitalMicrograph software) over 5–15 min.

We first surveyed C_{60} encapsulated in CNTs on the screen at 200,000× magnification to identify CNTs for reaction monitoring. Having found bundles of CNTs suitable for kinetic studies, we stopped the beam irradiation and changed the magnification to 800,000×. After waiting for 1 min, until thermal drift of the grid ceased or it was at least relatively relaxed, we commenced observation and movie recording. Focusing was carried out during the collection of images, which was recorded at slightly under-focus conditions (defocus value 10–20 nm). At 80, 100, and 120 kV, we continuously focused on 25–70 molecules in total, with a frame rate of 1.0 s for 5–15 min, until most of the C_{60} molecules oligomerized to form an inner nanotube. At 60 kV, the recording time was set to be 15–20 min, following the results of kinetic studies at 80 kV.

Temperature control The temperatures were controlled by using a heating holder (JEOL EM-21130). The accuracy of the grid temperature was 2–3 degrees (according to the instrument specifications). After the stage temperature was raised to the setting value, we waited at least 30 min before commencing observations, in order to stabilize the stage for minimization of thermal drift.

Image processing The images were collected as a .dm3 or .dm4 format file on Gatan DigitalMicrograph software and processed using ImageJ 1.47t software for .dm3 files.[54]

Visual data analysis for counting reaction events of C_{60} dimerization The products of C_{60} dimerization were visually identified following a protocol described in a previous report,[19] where molecular structures of [2 + 2] cycloadducts were studied thoroughly using atomic-resolution TEM imaging combined with TEM simulations. The progress of the reactions was studied by analyzing the movies backward, from the end of the reaction, to identify C_{60} dimerization. This procedure eliminates complications due to the intervention of equilibrium caused by thermal cycloreversion. The kinetics of cycloaddition between the fused dimer of C_{60} molecules and C_{60} was excluded from the analysis because the resultant product could possess very different properties.

ASSOCIATED CONTENT

Supporting Information

The Supporting Information is available free of charge on the ACS Publications website. Experimental procedures, physical properties of the compounds, additional spectra, and characterization data (PDF).

AUTHOR INFORMATION

Corresponding Author

*Correspondence to: muro@chem.s.u-tokyo.ac.jp, harano@chem.s.u-tokyo.ac.jp, nakamura@chem.s.u-tokyo.ac.jp

Notes

REFERENCES

(1) Knoll, M.; Ruska, E. Das Elektronenmikroskop. *Z. Phys.* **1932**, *78*, 318–339.

(2) Williams, D. B.; Carter, C. B. Inelastic Scattering and Beam Damage. In *Transmission Electron Microscopy: A Textbook for Materials Science*; Williams, D. B., Carter, C. B., Eds.; Springer US: Boston, MA, 2009.

(3) Egerton, R. F. Radiation Damage to Organic and Inorganic Specimens in the TEM. *Micron* **2019**, *119*, 72–87.

(4) Cai, Z.; Chen, S.; Wang, L.-W. Dissociation Path Competition of Radiolysis Ionization-Induced Molecule Damage under Electron Beam Illumination. *Chem. Sci.* **2019**, *10*, 10706–10715.

(5) Liu, Z.; Yanagi, K.; Suenaga, K.; Kataura, H.; Iijima, S. Imaging the Dynamic Behaviour of Individual Retinal Chromophores Confined inside Carbon Nanotubes. *Nat. Nanotechnol.* **2007**, *2*, 422–425.

(6) Okazaki, T.; Iizumi, Y.; Okubo, S.; Kataura, H.; Liu, Z.; Suenaga, K.; Tahara, Y.; Yudasaka, M.; Okada, S.; Iijima, S. Coaxially Stacked Coronene Columns inside Single-Walled Carbon Nanotubes. *Angew. Chem., Int. Ed.* **2011**, *50*, 4853–4857.

(7) Chamberlain, T. W.; Biskupek, J.; Skowron, S. T.; Bayliss, P. A.; Bichoutskaia, E.; Kaiser, U.; Khlobystov, A. N. Isotope Substitution Extends the Lifetime of Organic Molecules in Transmission Electron Microscopy. *Small* **2015**, *11*, 622–629.

(8) Harano, K.; Takenaga, S.; Okada, S.; Niimi, Y.; Yoshikai, N.; Isobe, H.; Suenaga, K.; Kataura, H.; Koshino, M.; Nakamura, E. Conformational Analysis of Single Perfluoroalkyl Chains by Single-Molecule Real-Time Transmission Electron Microscopic Imaging. *J. Am. Chem. Soc.* **2014**, *136*, 466–473.

(9) Iizumi, Y.; Liu, Z.; Suenaga, K.; Okada, S.; Higashibayashi, S.; Sakurai, H.; Okazaki, T. Molecular Arrangements of Corannulene and Sumanene in Single-Walled Carbon Nanotubes. *ChemNanoMat* **2018**, *4*, 557–561.

(10) Nakamura, E. Atomic-Resolution Transmission Electron Microscopic Movies for Study of Organic Molecules, Assemblies, and Reactions: The First 10 Years of Development. *Acc. Chem. Res.* **2017**, *50*, 1281–1292.

(11) Harano, K.; Minami, K.; Noiri, E.; Okamoto, K.; Nakamura, E. Protein-Coated Nanocapsules via Multilevel Surface Modification. Controlled Preparation and Microscopic Analysis at Nanometer Resolution. *Chem. Commun.* **2013**, *49*, 3525–3527.

(12) Palotás, J.; Negyedi, M.; Kollarics, S.; Bojtor, A.; Rohringer, P.; Pichler, T.; Simon, F. Incidence of Quantum Confinement on Dark Triplet Excitons in Carbon Nanotubes. *ACS Nano* **2020**, *14*, 11254–11261.

(13) Pichler, T.; Knupfer, M.; Golden, M. S.; Fink, J.; Rinzler, A.; Smalley, R. E. Localized and Delocalized Electronic States in Single-Wall Carbon Nanotubes. *Phys. Rev. Lett.* **1998**, *80*, 4729–4732.

(14) Sato, Y.; Terauchi, M. High-Energy Resolution Electron Energy-Loss Spectroscopy Study of Interband Transitions Characteristic to Single-Walled Carbon Nanotubes. *Microsc. Microanal.* **2014**, *20*, 807–814.

(15) Börner, P.; Kaiser, U.; Lehtinen, O. Evidence against a Universal Electron-Beam-Induced Virtual Temperature in Graphene. *Phys. Rev. B* **2016**, *93*, 134104.

(16) Susi, T.; Meyer, J. C.; Kotakoski, J. Quantifying Transmission Electron Microscopy Irradiation Effects Using Two-Dimensional Materials. *Nat. Rev. Phys.* **2019**, *1*, 397–405.

(17) Smith, B. W.; Monthioux, M.; Luzzi, D. E. Encapsulated C_{60} in Carbon Nanotubes. *Nature* **1998**, *396*, 323–324..

(18) Koshino, M.; Niimi, Y.; Nakamura, E.; Kataura, H.; Okazaki, T.; Suenaga, K.; Iijima, S. Analysis of the Reactivity and Selectivity of Fullerene Dimerization Reactions at the Atomic Level. *Nat. Chem.* **2010**, *2*, 117–124.

(19) Okada, S.; Kowashi, S.; Schweighauser, L.; Yamanouchi, K.; Harano, K.; Nakamura, E. Direct Microscopic Analysis of Individual C_{60} Dimerization Events: Kinetics and Mechanisms. *J. Am. Chem. Soc.* **2017**, *139*, 18281–18287..

(20) Koshino, M.; Tanaka, T.; Solin, N.; Suenaga, K.; Isobe, H.; Nakamura, E. Imaging of Single Organic Molecules in Motion. *Science* **2007**, *316*, 853–853.

(21) Nakamura, E.; Koshino, M.; Tanaka, T.; Niimi, Y.; Harano, K.; Nakamura, Y.; Isobe, H. Imaging of Conformational Changes of Biotinylated Triamide Molecules Covalently Bonded to a Carbon Nanotube Surface. *J. Am. Chem. Soc.* **2008**, *130*, 7808–7809.

(22) Hanayama, H.; Yamada, J.; Tomotsuka, I.; Harano, K.; Nakamura, E. Rim Binding of Cyclodextrins in Size-Sensitive Guest Recognition. *J. Am. Chem. Soc.* **2021**, *143*, 5786–5792.

(23) Xing, J.; Schweighauser, L.; Okada, S.; Harano, K.; Nakamura, E. Atomistic Structures and Dynamics of Prenucleation Clusters in MOF-2 and MOF-5 Syntheses. *Nat. Commun.* **2019**, *10*, 3608.

(24) Nakamuro, T.; Sakakibara, M.; Nada, H.; Harano, K.; Nakamura, E. Capturing the Moment of Emergence of Crystal Nucleus from Disorder. *J. Am. Chem. Soc.* **2021**, *143*, 1763–1767.

(25) Egerton, R. F. Radiation Damage and Nanofabrication in TEM and STEM. *Microscopy Today* **2021**, *29*, 56–59.

(26) Turro, N. J.; Ramamurthy, V.; Scaiano, J. C. *Principles of Molecular Photochemistry: An Introduction*.; University Science Books: 2009.

(27) Ohmori, N.; Suzuki, T.; Ito, M. Why Does Intersystem Crossing Occur in Isolated Molecules of Benzaldehyde, Acetophenone, and Benzophenone? *J. Phys. Chem.* **1988**, *92*, 1086–1093.

(28) May, V.; Kühn, O. Charge and Energy Transfer Dynamics in Molecular Systems, 3rd revised and enlarged ed.; Wiley-VCH; 2011.

(29) Inokuti, M. Inelastic Collisions of Fast Charged Particles with Atoms and Molecules---The Bethe Theory Revisited.

Rev. Mod. Phys. **1971**, *43*, 297–347.

(30) Allan, M. Study of Triplet States and Short-Lived Negative Ions by Means of Electron Impact Spectroscopy. *J. Electron Spectrosc. Relat. Phenom.* **1989**, *48*, 219–351.

(31) Carlson, L. J.; Krauss, T. D. Photophysics of Individual Single-Walled Carbon Nanotubes. *Acc. Chem. Res.* **2008**, *41*, 235–243.

(32) Bandow, S.; Takizawa, M.; Hirahara, K.; Yudasaka, M.; Iijima. S. Raman Scattering Study of Double-Wall Carbon Nanotubes Derived from the Chains of Fullerenes in Single-Wall Carbon Nanotubes. *Chem. Phys. Lett.* **2001**, *337*, 48–54.

(33) Rao, A. M.; Zhou, P.; Wang, K.-A.; Hager, G. T.; Holden, J. M.; Wang, Y.; Lee, W.-T.; Bi, X.-X.; Eklund, P. C.; Cornett, D. S.; Duncan, M. A.; Amster, I. J. Photoinduced Polymerization of Solid C_{60} Films. *Science* **1993**, *259*, 955–957.

(34) Wang, Y.; Holden, J. M.; Dong, Z.-H.; Bi, X.-X.; Eklund, P. C. Photo-Dimerization Kinetics in Solid C_{60} Films. *Chem. Phys. Lett.* **1993**, *211*, 341–345.

(35) Han, S.; Yoon, M.; Berber, S.; Park, N.; Osawa, E.; Ihm, J.; Tománek, D. Microscopic Mechanism of Fullerene Fusion. *Phys. Rev. B* **2004**, *70*, 113402.

(36) Kaiser, U.; Biskupek, J.; Meyer, J. C.; Leschner, J.; Lechner, L.; Rose, H.; Stöger-Pollach, M.; Khlobystov, A. N.; Hartel, P.; Müller, H.; Haider, M.; Eyhusen, S.; Benner, G. Transmission Electron Microscopy at 20 KV for Imaging and Spectroscopy. *Ultramicroscopy* **2011**, *111*, 1239–1246.

(37) Mirzayev, R.; Mustonen, K.; Monazam, M. R. A.; Mittelberger, A.; Pennycook, T. J.; Mangler, C.; Susi, T.; Kotakoski, J.; Meyer, J. C. Buckyball Sandwiches. *Sci. Adv.* **2017**, *3*, e1700176.

(38) Jordan, J. W.; Fung, K. L. Y.; Skowron, S. T.; Allen, C. S.; Biskupek, J.; Newton, G. N.; Kaiser, U.; Khlobystov, A. N. Single-Molecule Imaging and Kinetic Analysis of Intermolecular Polyoxometalate Reactions. *Chem. Sci.* **2021**, *12*, 7377–7387.

(39) Laidler, K. J. Elementary Gas-Phase Reactions. In *Chemical Kinetics*, 3rd ed.; Prentice Hall: 1987.

(40) Shimizu, T.; Lungerich, D.; Stuckner, J.; Murayama, M.; Harano, K.; Nakamura, E. Real-Time Video Imaging of Mechanical Motions of a Single Molecular Shuttle with Sub-Millisecond Sub-Angstrom Precision. *Bull. Chem. Soc. Jpn.* **2020**, *93*, 1079–1085.

(41) Fraelich, M. R.; Weisman, R. B. Triplet States of Fullerene C_{60} and C_{70} in Solution: Long Intrinsic Lifetimes and Energy Pooling. *J. Phys. Chem.* **1993**, *97*, 11145–11147.

(42) Bunker, D. L.; Hase, W. L. On non-RRKM unimolecular kinetics: Molecules in general, and CH_3NC in particular *J.*

Chem. Phys. **1973**, *59*, 4621−4632.

(43) Yomogida, Y.; Tanaka, T.; Zhang, M.; Yudasaka, M.; Wei, X.; Kataura, H. Industrial-Scale Separation of High-Purity Single-Chirality Single-Wall Carbon Nanotubes for Biological Imaging. *Nat. Commun.* **2016**, *7*, 12056.

(44) Wepasnick, K. A.; Smith, B. A.; Schrote, K. E.; Wilson, H. K.; Diegelmann, S. R.; Fairbrother, D. H. Surface and Structural Characterization of Multi-Walled Carbon Nanotubes Following Different Oxidative Treatments. *Carbon* **2011**, *49*, 24–36.

(45) Kim, U. J.; Furtado, C. A.; Liu, X.; Chen, G.; Eklund, P. C. Raman and IR Spectroscopy of Chemically Processed Single-Walled Carbon Nanotubes. *J. Am. Chem. Soc.* **2005**, *127*, 15437–15445.

(46) Chen, C.-Y.; Zepp, R. G. Probing Photosensitization by Functionalized Carbon Nanotubes. *Environ. Sci. Technol.* **2015**, *49*, 13835–13843.

(47) Urita, K.; Suenaga, K.; Sugai, T.; Shinohara, H.; Iijima, S. In Situ Observation of Thermal Relaxation of Interstitial-Vacancy Pair Defects in a Graphite Gap *Phys. Rev. Lett.* **2005**, *94*, 155502.

(48) Zobač, V.; Lewis, J. P.; Abad, E.; Mendieta-Moreno, J. I.; Hapala, P.; Jelínek, P.; Ortega, J. Photo-Induced Reactions from Efficient Molecular Dynamics with Electronic Transitions Using the FIREBALL Local-Orbital Density Functional Theory Formalism. *J. Phys.: Condens. Matter* **2015**, *27*, 175002.

(49) Yu, H.; Jin, Y.; Peng, F.; Wang, H.; Yang, J. Kinetically Controlled Side-Wall Functionalization of Carbon Nanotubes by Nitric Acid Oxidation. *J. Phys. Chem. C* **2008**, *112*, 6758–6763.

(50) Sakai, M.; Ichida, M.; Nakamura, A. Raman Scattering Study of Photopolymerization Kinetics in C_{60} Crystals. *Chem. Phys. Lett.* **2001**, *335*, 559–566.

(51) Hashiguchi, M.; Inada, H.; Matsuo, Y. Solution-Phase Synthesis of Dumbbell-Shaped C_{120} by $FeCl_3$-Mediated Dimerization of C_{60}. *Carbon* **2013**, *61*, 418–422.

(52) Egerton, R. F.; Takeuchi, M. Radiation Damage to Fullerite (C_{60}) in the Transmission Electron Microscope. *Appl. Phys. Lett.* **1999**, *75*, 1884–1886.

(53) Pangborn, A. B.; Giardello, M. A.; Grubbs, R. H.; Rosen, R. K.; Timmers, F. J. Safe and Convenient Procedure for Solvent Purification. *Organometallics* **1996**, *15*, 1518–1520.

(54) Schneider, C. A.; Rasband, W. S.; Eliceiri, K. W. NIH Image to ImageJ: 25 Years of Image Analysis. *Nat. Methods* **2012**, *9*, 671–675.

E-beam catalysis in [2 + 2] cycloaddition

CNT   S exciton $(C_{60})_2$@prCNT